Supercells and Tornado-like Vortices in an Idealized Global Atmosphere Model

Kai-Yuan Cheng[1,2], Shian-Jiann Lin[3], Lucas Harris[2], and Linjiong Zhou[1,2]

[1]Program in Oceanic and Atmospheric Sciences, Princeton University, Princeton, NJ, USA.

[2]NOAA/Geophysical Fluid Dynamics Laboratory, Princeton, NJ, USA.

[3]Tianji Meteorological Sciences and Technology Inc., Beijing, China.

Corresponding author: Kai-Yuan Cheng (kai-yuan.cheng@noaa.gov)

Key Points:

- A stretched-grid global model can realistically simulate individual supercells and cloudy tornado-like vortices at kilometer scales
- The vortex is initiated and maintained by the updraft core by tilting the near-ground environmental horizontal vorticity vertically
- The dynamics of the vortices is consistent with previous studies on tornadogenesis

Abstract

We investigate the representation of individual supercells and intriguing tornado-like vortices in a simplified, locally-refined global atmosphere model. The model, featuring grid stretching, can locally enhance the model resolution and economically reach the cloud-resolving scale. Given an unstable sheared environment, the model can simulate supercells realistically, with a near-ground vortex and funnel cloud at the center of a rotating updraft reminiscent of a tornado. An analysis of the vorticity budget suggests that the updraft core of the supercell tilts environmental horizontal vorticity into the tornado-like vortex. The updraft also acts to amplify the vortex through vertical stretching. Results suggest that the simulated vortex is dynamically similar to observed tornadoes and modeling studies at much higher horizontal resolution.

Plain Language Summary

We use a simplified global model to study individual supercells and intriguing cloudy vortices that behave like tornadoes. This model incorporates grid-stretching techniques, making it a cost-effective tool to study supercells on a full-size Earth. The model can realistically simulate supercells and cloudy tornado-like vortices even at kilometer scales, which appears unprecedented in the literature. We find that the physics behind the vortices is consistent with previous studies, including observations of tornadogenesis and simulations at much higher resolution.

1 Introduction

A supercell (an intense convective storm characterized by a single quasi-steady rotating updraft) is often associated with severe weather for its capabilities of producing destructive winds, large hailstones, extreme precipitation, and dangerous tornadoes. Many field campaigns, such as RELAMPAGO (Remote sensing of Electrification, Lightning, And Mesoscale/microscale Processes with Adaptive Ground Observations; Nesbitt et al. 2021) and VORTEX2 (Verification of the Origins of Rotation in Tornadoes Experiment 2; Wurman et al., 2012), provide invaluable datasets for understanding the processes associated with supercells. Those observations, however, are subject to the field of view for a remote sensing device or sample size for an in-situ instrument. On the other hand, a numerical model can provide a comprehensive picture of a supercell, i.e., all variables at every grid cell within a computational domain.

Historically, simulations of supercells were feasible only in limited-area domains (e.g., Klemp & Wilhelmson, 1978; Schlesinger, 1978; Wang et al., 2016; Orf et al., 2016) due to the cost of both high temporal and spatial resolutions that are required to resolve supercells. These limited-area models limit the ability for the simulated storm to interact with its larger-scale environment. Nowadays, because of continuous advances in computational capacity, the atmospheric sciences community is ushering in a new era of global cloud-resolving models.

Several numerical modeling centers are working on the development of global cloud-resolving models with 2-5 km horizontal resolution that can explicitly resolve deep convection (Satoh et al., 2019; Stevens et al., 2019; Cheng et al. 2022). The ability of a global model to represent deep convection not only reduces the uncertainty caused by cumulus parameterizations (e.g., Stevens & Bony, 2013), but it also paves the way toward a better understanding of multiscale interaction involving convection (e.g., Madden-Julian Oscillation and cloud feedback; Zavadoff et al. 2023). While this new class of global models has been proven useful for understanding the properties of intense convection on a global scale (Cheng et al., 2022; Harris et al., 2023), these models are at best marginally able to accurately simulate individual supercells. In fact, this group of global models is referred to as global storm-resolving models in numerous studies (e.g., Judt et al., 2021; Nugent et al., 2022).

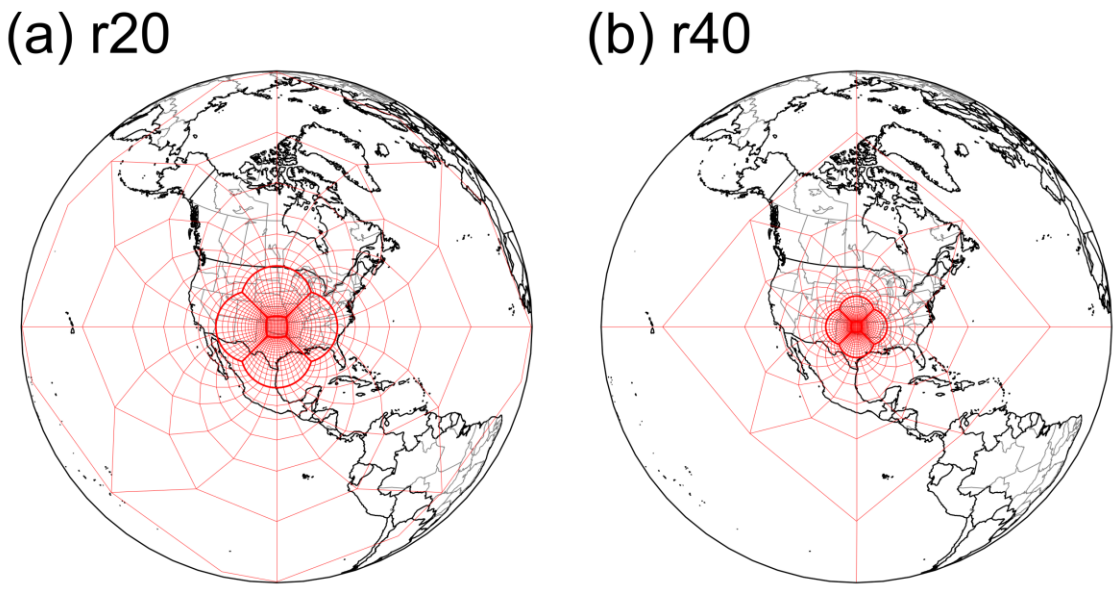

Figure 1. Illustration of two stretched grid configurations for a C512 cubed-sphere grid. Grids are shown by light red lines and the cubed-sphere edges are shown by heavy red lines. Each grid box represents 64 by 64 actual grid cells. (a) r20 configuration, the finest grid spacing is about 1 km; (b) r40, ~500 m. Borders, countries, and states are plotted as a reference scale for demonstration purposes.

In this study, we describe an efficient nonhydrostatic global model using grid stretching, and conduct idealized simulations of a supercell at various resolutions on cloud-resolving scales, ranging from 4 km down to 500 m. The configuration of the simulation is similar to the supercell

test case used in the 2016 Dynamical Core Model Intercomparison Project (DCMIP2016; Ullrich et al., 2017; Zarzycki et al., 2019). Unlike the DCMIP2016 simulations that were conducted on a small Earth with its radius reduced by a factor of 120, our simulations are conducted on a full-size Earth. Figure 1 shows examples of the grid configurations used in this study. Our model features grid-stretching, which can reach cloud-resolving scales while requiring less than one one-thousandth of the computational resources that would be needed for the simulation to be performed at the same resolution globally. Our model can realistically simulate individual supercells and even intriguing vortices that develop near the ground and are qualitatively similar to tornadoes. We refer to those vortices as "tornado-like vortices", analogous to the so-called "tropical cyclone-like vortices" in 20-100 km global models (e.g., Zhao et al., 2012). We believe that this is the first time such vortices have ever been simulated in a full-size Earth global model.

2 Model Description and Simulation Design

An idealized nonhydrostatic global model that can reach the cloud-resolving scale locally is developed for this study. The model is powered by the finite-volume cubed-sphere dynamical core (FV3) developed at the Geophysical Fluid Dynamics Laboratory (GFDL). The dynamical core solves the vector-invariant Euler equations for atmospheric motions using the C-D grid algorithm of Lin & Rood (1997) on a gnomonic cubed-sphere (Putman & Lin, 2007) and a Lagrangian vertical coordinate (Lin, 2004). The pressure gradient force is solved by the finite-volume algorithm of Lin (1997). The nonhydrostatic component is handled by a vertically semi-implicit scheme described in Harris et al. (2020). For physics parameterization, we use the GFDL microphysics scheme, version 3 (Zhou et al., 2022) with warm-rain processes only for simplicity, which has been previously used in the study of anvil cloud fraction (Jeevanjee and Zhou, 2022). They found that the warm-rain only and the full microphysics produce similar cloud structures.

FV3 can refine the cubed-sphere by an analytical "stretching" (Schmidt 1977; Harris et al., 2016), which allows it to enhance the resolution locally down to cloud-resolving scales and even finer. For this study, four configurations of the cubed-sphere grid are used to achieve different horizontal resolutions. A cubed-sphere with 128 × 128 (C128) and 256 × 256 (C256) cells on each face is stretched by a factor of 20 to reach minimum grid-cell widths of 4 and 2 km, respectively. A cubed-sphere with 512 × 512 (C512) cells on each face is stretched by a factor of 20 and 40 to reach minimum grid-cell widths of 1 km and 500 m, respectively. Figure 1 shows

examples of stretched C512 cubed-sphere grids in the 1 km and 500 m cases. The center of the high-resolution region is placed at 35.4° N and 262.4° W for demonstration purposes. The location of the high-resolution region has no effect on the solution since the Earth's rotation is turned off. The grid configurations are summarized in Table 1. All simulations use 90 vertical levels with a top at 50 hPa. The vertical layer thickness is finest at the bottom level (~8 m) and gradually expands with height.

Resolution (km)	Cubed-sphere resolution	Grid-stretching factor	Acoustic timestep (s)
4	128	20	5.0
2	256	20	2.5
1	512	20	1.25
0.5	512	40	0.625

Table 1. Configuration of grid and timestep for each simulation.

All simulations are initialized using the environment of Toy (2012) with modifications. This environment is favorable for the development of supercells. The thermodynamic profile is adapted from Weisman and Klemp (1982). The environment has a convective available potential energy of 2515 J·kg^{-1}. For the wind profile (U and V in a local Cartesian system), an analytic approximation of Toy's profile is used:

$$U(z) = 15\,\mathrm{m\cdot s^{-1}}\left[1+\tanh\left(\frac{z-3\,\mathrm{km}}{2\,\mathrm{km}}\right)\right]-8.5\,\mathrm{m\cdot s^{-1}}$$
$$V(z) = 8.5\,\mathrm{m\cdot s^{-1}}\left[\tanh\left(\frac{z}{1\,\mathrm{km}}\right)-0.5\right], \quad (1)$$

where z is the altitude in km.

The wind profile is then mapped onto a spherical domain (u and v in a spherical coordinate system) by multiplying a horizontal Gaussian:

$$u(\lambda,\theta,z) = U(z)\,exp\left(-\frac{8D}{R_e}\right), \quad (2)$$

and similarly for $v(\lambda,\theta,z)$, where λ and θ are longitude and latitude, respectively; D is the great-circle distance from the center of the high-resolution region; R_e is the radius of the Earth.

The model uses a warm bubble to initiate convection. For all simulations, the thermal perturbation of the warm bubble is 2 K. The radial dimension of the bubble is 10 km in the

horizontal direction and 1.4 km in the vertical direction. All four simulations are integrated for 2 hours with the same physics timestep of 5 s. The acoustic timestep varies with different resolutions and is tabulated in Table 1.

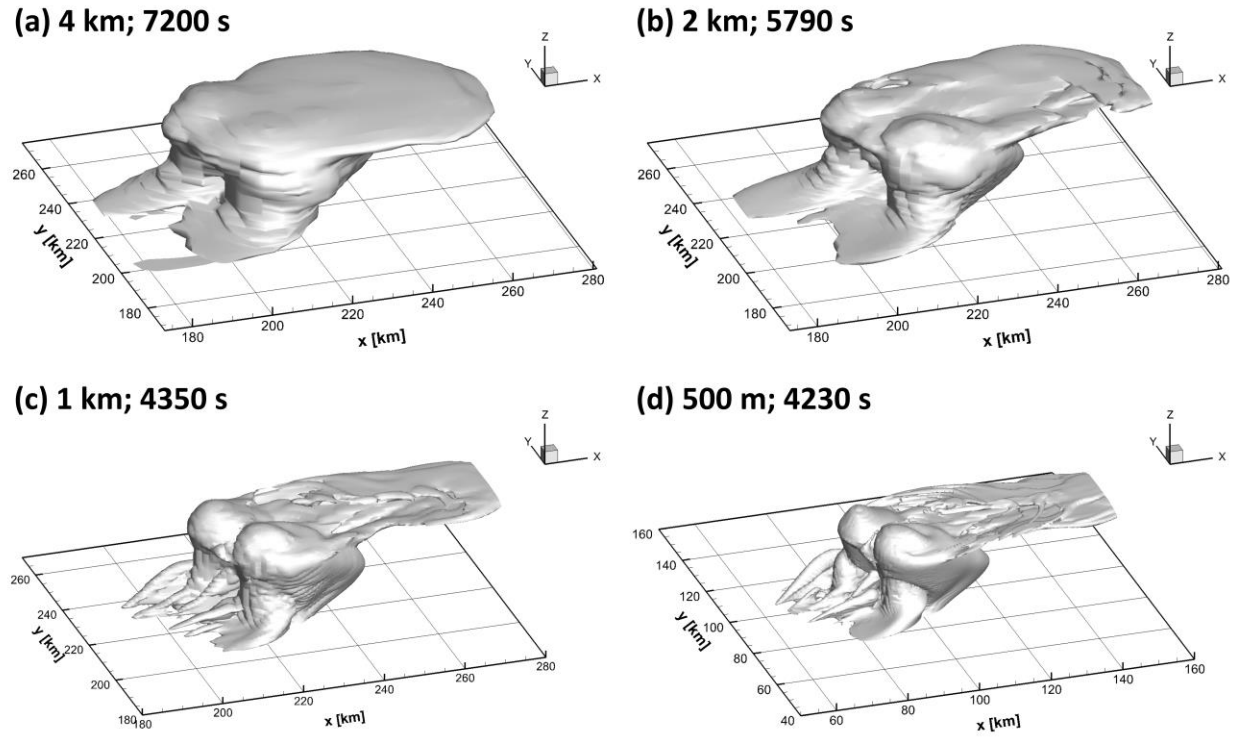

Figure 2 Perspective view of a supercell in its mature stage for the (a) 4 km, (b) 2 km, (c) 1 km, and (d) 500 m simulations. The white isosurface depicts the appearance of the supercell, which is defined by 0.1 g·kg^{-1} in total hydrometeor q_l (a combination of cloud water q_c and rainwater q_r). The simulation time of the snapshot is indicated.

3 Supercell in a Global Model

Our global model is capable of simulating an individual supercell realistically at all four resolutions considered. Despite having varied horizontal resolutions, all simulated supercells show similarities in terms of storm morphology. After initialization, the supercell goes through the cumulus stage and persists in the mature stage. Figure 2 shows the appearance of the supercell in its mature stage at different resolutions. Common storm features can be seen, including protruding overshooting tops and a wide-spreading anvil. All simulations have a storm

of similar dimensions: about 40 km in both *x* and *y* directions. As for the vertical dimension, the storm in each simulation can grow over the height of 15 km. Such similarity in the dimension is a result of the same warm bubble used to initialize the simulations. At higher resolutions, expectedly, the supercell's appearance becomes more complicated, as turbulent motions at small scales are better resolved. The overshooting top becomes more prominent, and the anvil shows more wave structures. Also, the supercell at a higher resolution tends to grow faster with more intense updrafts than that at a lower resolution. Such dependencies on grid spacing are consistent with previous studies (e.g., Noda & Niino, 2003; Potvin & Flora, 2015).

It is worth noting that the supercell in all cases is splitting, which is intrinsic storm dynamics given the vertically veered low-level wind profile. The behavior of storm splitting is consistent with previous studies using similar wind profiles (e.g., Toy, 2012; Weisman & Rotunno, 2000). At a higher resolution, the splitting occurs more quickly and prominently. One possible explanation is that the vortex dynamics and pressure perturbations are better resolved at a higher resolution, which plays an important role in the storm splitting.

Next, we examine the dynamics of the simulated supercell, focusing on the stronger right-moving (clockwise-rotating) cell. Figure 3 shows the horizontal distribution of vertical vorticity ζ, vertical velocity w, and q_l in all simulations. ζ and q_l are from the level near the ground (~27 m AGL), while w is from another level aloft (~1.74 km AGL). ζ and w are used to illustrate the dynamics of the supercell whereas q_l is used to depict the shape of the supercell. From q_l distribution, it can be seen that the supercell in all cases gets twisted by the clockwise hodograph curvature (Equation 1). At higher resolutions, the bending of the storm becomes more prominent. All simulations, except for the 4 km case, show a hook-shaped pattern, resembling the hook echo radar signature of a supercell. In particular, the hook-shaped pattern is well-resolved in the 1 km and 500 m simulations. A hook echo signature is a useful indication of tornadogenesis, as discussed by many studies (e.g., Markowski, 2002). Indeed, all simulations, except for 4 km, have "tornado-like" vortices forming near the ground. We will examine those vortices in detail and discuss their formation in the following section.

In addition to the hook-shaped pattern, common storm structures such as forward flank downdraft (FFD) and rear flank downdraft (RFD) can be seen in Figure 3, especially in the high-resolution simulations (1 km and 500 m). Take the 1 km simulation for example (Figure 3c), an FFD is shown by a region of strong and well-organized downdrafts, primarily generated by

precipitation loading and evaporative cooling, north to the main updraft at x = 220.0 km and y = 216.0 km. An RFD develops west to the main updraft around x = 210.0 km and y = 205.0 km (roughly outlined by the zero contour of w), a weak and loosely defined downdraft is forced primarily by vertical pressure gradient.

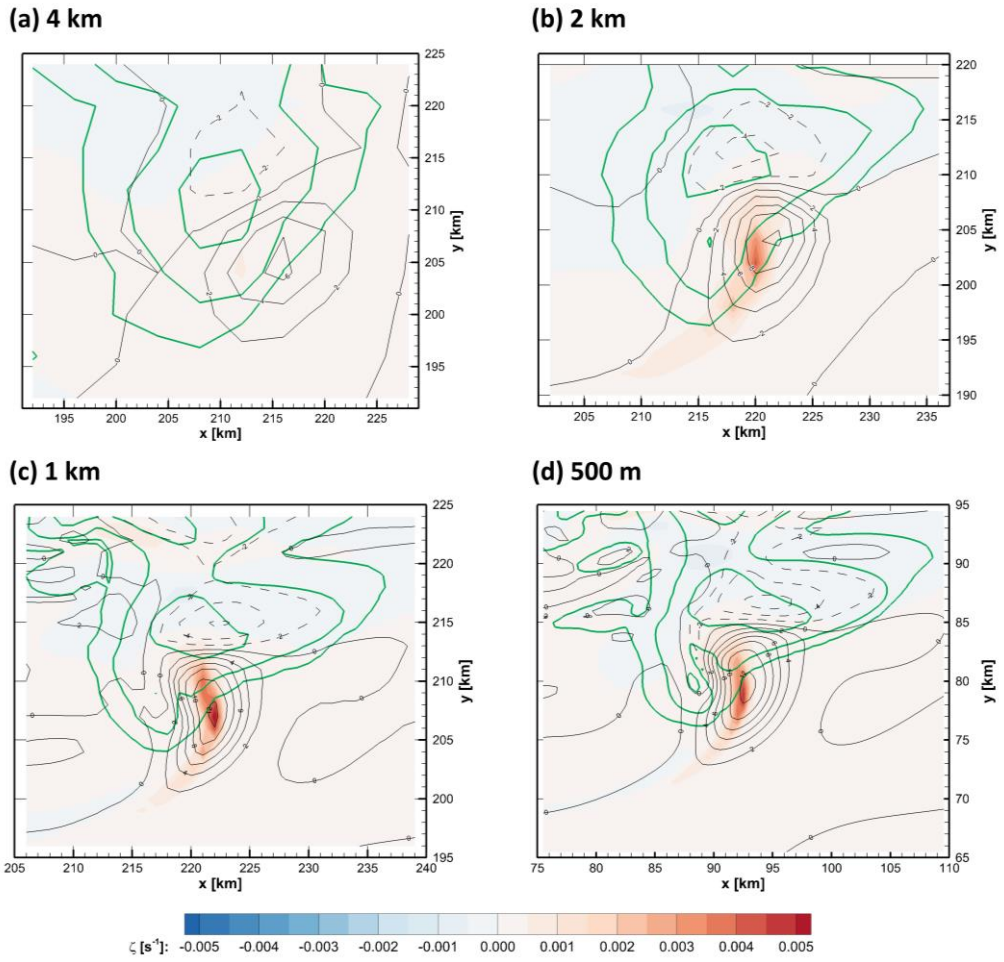

Figure 3. Dynamical structure of the clockwise-rotating right-moving cell in the mature stage in (a) 4 km, (b) 2 km, (c) 1 km, and (d) 500 m simulations at the same time as in Figure 2. Color shading and green contours are w and q_l, respectively, near the ground (~27 m AGL). The q_l contours are 0.1, 1.0, and 5.0 g·kg^{-1}. Black contours show w at an AGL of ~1.74 km. The w contour interval is 2 m s^{-1}, with negative contours dashed.

The storm morphology and the dynamical features are consistent with previous observational and theoretical studies (e.g., Figure 2 in Davies-Jones, 2015). In the 4-km

simulation, the overshooting top, RFD, and FFD are not as prominent as in other cases at a higher resolution. Nevertheless, the dynamics of the supercell in the 4-km simulation are qualitatively similar to that in the high-resolution ones. The result indicates that our global model is capable of reproducing a supercell storm realistically.

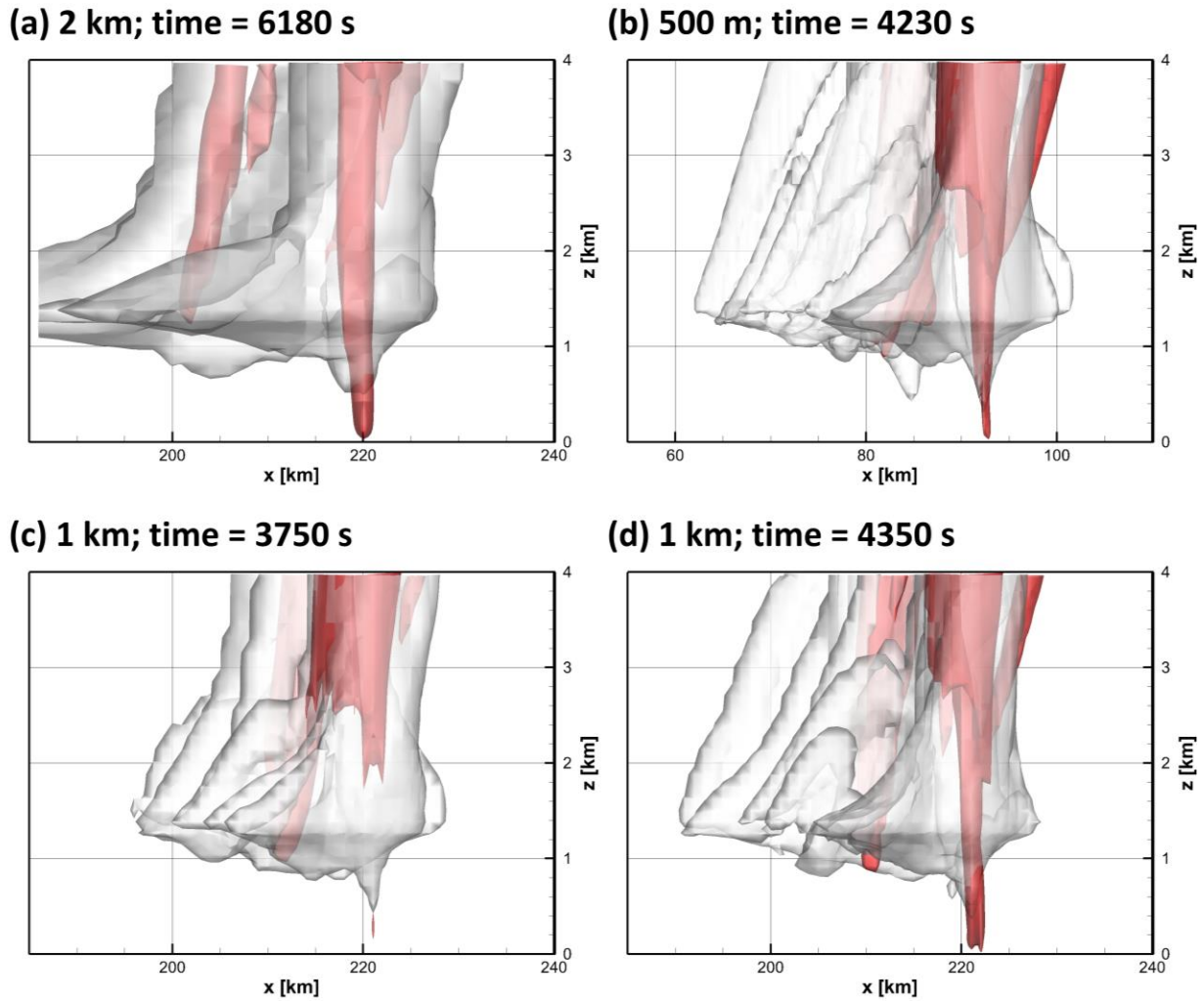

Figure 4. Development of cloudy tornado-like vortex. (a) 6180 s in 2 km, (b) 4230 s in 500 m, (c) 3750 s and (d) 4350 s in 1 km simulation. The solid red isosurface is $\zeta = 0.005\ s^{-1}$, while the transparent white isosurface is $q_c = 0.1\ g \cdot kg^{-1}$.

4 Tornado-like Vortex

In this section, we report and discuss the existence of an intriguing cloudy vortex that develops near the ground in all cases except for the 4 km (Figures 3 and 4). As the vortices in those three simulations are similar physically, we use the 1 km simulation only to illustrate the

physics and formation of the vortex. The horizontal distribution of ζ near the ground in the 1 km simulation can be seen in Figure 3c. A strong ζ is developing locally at x = 222.0 km and y = 207.0 km, near the hook-shaped pattern in q_l discussed previously. The strong ζ is a horizontal cross-section of a 3-D vortex. Figure 4c and d show the development of the cloudy vortex near the ground. At 3750 s into the simulation, where the supercell is in its mature stage, a local ζ is developing at x = 221.0 km and z = 0.3 km and forming a vertically-extending vortex just below the downward extruding cloud, outlined by the white isosurface of q_c, at the bottom of the supercell (Figure 4c). The extruding cloud resembles a funnel cloud that is often, but not always, a visual precursor of a tornado. As time goes on, the vortex intensifies and extends further both upward and downward, forming a long vortex from the ground all the way to the middle levels inside the supercell (Figure 4d). Also, the funnel cloud expands a bit. This cloudy vortex is long-lasting and evolving towards the end of the simulation. The vortex has a width of ~ 3 km in the 1 km simulation. The vortex in the 2 km case has a comparable size and that in the 500 m case is slightly thinner. These vortices are much wider than a typical tornado (hundreds of meters) but comparable to the widest "wedge" tornadoes, such as the 5-km wide tornado studied by Wurman et al. (2013). We refer to these cloudy vortices as "tornado-like vortices" hereafter, in analogy to the "tropical cyclone-like vortices" in 20-100 km global models (e.g., Zhao et al., 2012).

How did this funnel cloud form? Figure 5 shows the structure of the cloudy tornado-like vortex when it is fully developed (at the same moment as in Figure 4d). Near the ground (Figure 5a), an area of moist air (water vapor $q_v > 15$ g·kg^{-1}) forms in the forward flank of the supercell, which results from the evaporation of rainwater. This moist air can also be seen in a vertical cross-section cut through the cloudy vortex (Figure 5b). A region of saturated air forms near the ground in the y direction from 210 km to 215 km. This moist air then gets lifted into the rotating updraft, condenses water by adiabatic cooling, and forms the funnel cloud.

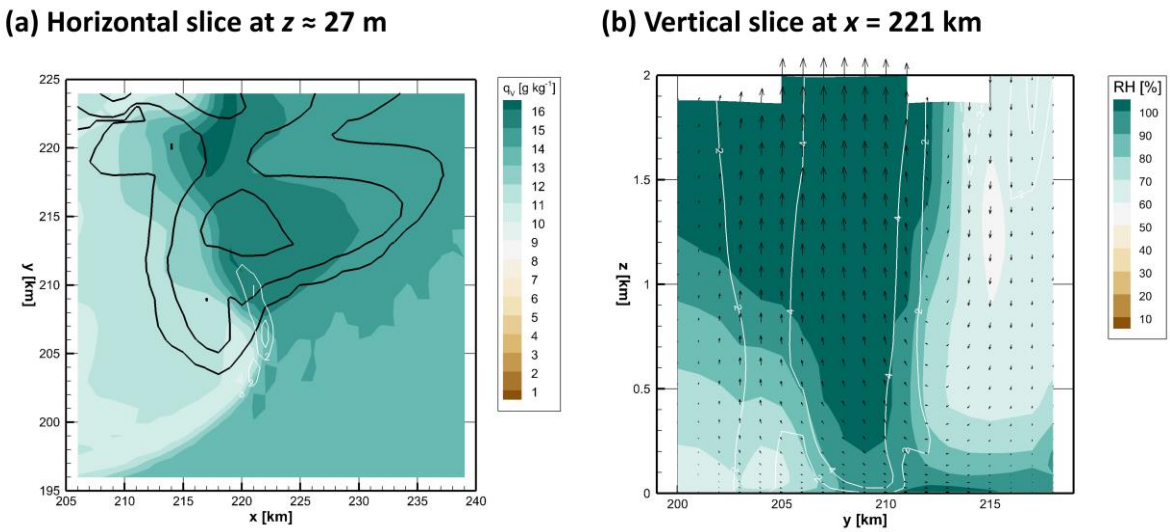

Figure 5 Structure of cloudy vortex at 4350 s in the 1 km simulation. (a) horizontal cross-section near the ground ($z \sim 27$ m). q_v is plotted in color shading. Black contours represent q_l of 0.1, 1.0, and 5.0 g·kg^{-1}. White contours represent ζ in the unit of 0.001 s^{-1}. (b) Vertical cross-section at x = 221 km. Relative humidity (RH) is plotted in color shading. White contours represent ζ, with negative contours dashed and zero contour omitted. Wind vectors are plotted in black.

Next, we examine the formation of the tornado-like vortex through the vorticity equation. The vertical vorticity equation in the height coordinates can be written as:

$$\frac{\partial \zeta}{\partial t} = -\nabla \cdot \vec{v}\zeta - \zeta\left(\frac{\partial u}{\partial x} + \frac{\partial v}{\partial y}\right) + \left(\frac{\partial w}{\partial y}\frac{\partial u}{\partial z} + \frac{\partial w}{\partial x}\frac{\partial v}{\partial z}\right) + \left(\frac{\partial p}{\partial x}\frac{\partial \alpha}{\partial y} + \frac{\partial p}{\partial y}\frac{\partial \alpha}{\partial x}\right), \quad (3)$$

where p and α are the pressure and specific density, respectively. Equation 3 describes that the local tendency of ζ is equal to, in order, advection, stretching, tilting, and baroclinicity.

We compute each of the four terms within the 1-km simulation. It turns out that the tilting and stretching terms play essential roles in forming the vortex, as has been found by numerous studies on tornadogenesis (Davies-Jones, 2015; Markowski & Richardson, 2009; Orf et al., 2016; Rotunno et al., 2017). Figure 6 shows the contribution from the tilting and stretching terms when the vortex starts to develop (the same moment as in Figure 4c). Beneath the vortex, the tilting term produces a positive ζ near the ground (Figure 6a). This positive ζ will get transported upward by the updraft. At the same time, the stretching term has a local maximum right at the developing tornado-like vortex near the ground (Figure 6b). The interpretation of Figure 6 is as follows. First, the tilting term initiates a positive ζ near the ground by redirecting the horizontal

vorticities (which results from the environmental vertical shear) through the horizontal gradient of vertical velocity (which results from the main updraft developed locally in the supercell). Second, the positive ζ is brought upward by the updraft core and gets intensified by the stretching term through convergence. Note that the stretching term cannot intensify or lessen ζ without a preexisting ζ. That is, the stretching term cannot create a positive/negative ζ from zero and only works to strengthen/weaken ζ. The effects that the tilting and stretching terms have on forming the tornado-like vortex are consistent with previous studies. It suggests that the simulated vortices, even though coarsely resolved, are dynamically the same as real-world tornadoes.

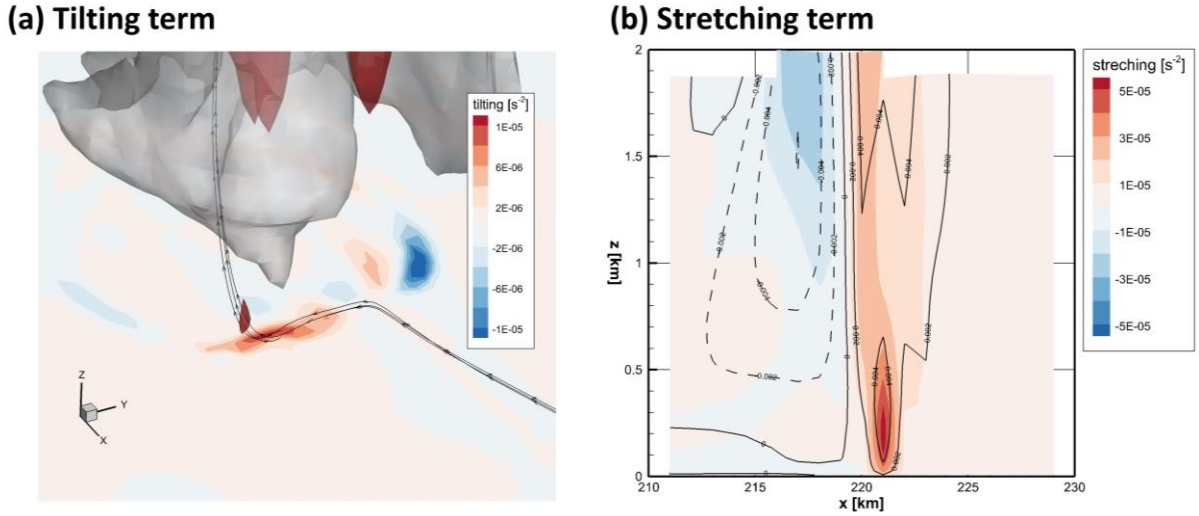

Figure 6. Two main contributors from the vorticity equation to the formation of the tornado-like vortex when the vortex is about to develop (3750 s) in the 1 km case. (a) tilting term in a 3-dimensional view. The solid red isosurface represents the tornado-like vortex (plotted by ζ = 0.005 s^{-1}), while the transparent white isosurface represents the funnel cloud (plotted by q_c = 0.1 $g \cdot kg^{-1}$). Color shading represents the contribution from the tilting term near the ground ($z \sim 27$ m). Streamlines through the vortex are plotted. (b) stretching term in an *xz* cross-section cut through the vortex (y = 209 km). Color shading represents the contribution from the stretching term. Line contours show vertical vorticities, with negative contours dashed.

The baroclinicity and advection do not appear to play an important role in forming the tornado-like vortex. The baroclinic term is at least one order of magnitude smaller than those

from the tilting and stretching terms near the vortex. The triviality of the baroclinic effect is discussed in both observational and theoretical papers (see section 3.2 in a review paper written by Davies-Jones, 2015). The advection term principally acts to move the vorticity maximum downstream.

5 Conclusions and Discussion

In the above, we present numerical simulations of a supercell storm at different resolutions on a full-size Earth using a newly developed global model. By utilizing a stretched global grid, the model can perform simulations on cloud-resolving scales using modest computational resources. The model is capable of producing a realistic supercell even at 4-km grid spacing. The storm morphology in all cases is consistent with observations and previous studies. It demonstrates a couple of interesting features of this simplified FV3-based model, including 1) a super-stretched global grid (up to a factor of 40) remains stable and accurate; 2) this setup could be a useful tool for process studies without the hassle of specifying lateral boundary conditions. It also shows the value of an FV3-based model for convective-storm simulation and prediction, which would apply equally well to regional contexts.

We found our simulated supercells also produced cloudy tornado-like vortices, which, to the best of our knowledge, have never before been simulated in the global modeling community. While wider than typical real-world tornadoes due to our grid cell sizes, the vortex is qualitatively similar to tornadoes: a funnel cloud with an intense vortex. It is found that, through analysis based on the vorticity equation, the tilting term initiates the vortices that are then intensified through stretching.

Previous modeling studies of tornadoes have used grid spacings of 50 m or smaller (Orf et al., 2017, and references therein). The capability of our model to produce tornado-like vortices at kilometer scales may reflect the strength of the D-grid staggering used in the FV3 dynamical core. On the D-grid, tangential winds are defined along grid boundaries, and so the circulation and thus by Stokes' Theorem cell-mean vorticity can be computed exactly. This may be the reason that our model can produce an intense vortex reminiscent of tornadoes even at kilometer scales, demonstrating the value of FV3's emphasis on vorticity dynamics.

Our model is capable of computing atmospheric flows and microphysics over a broad range of scales, ranging from tornado-like vortices to planetary waves. Our next step will be to take advantage of this capacity to study the cross-scale interactions involving supercells and

tornadoes. Gensini et al. (2019) studied the teleconnection between the U.S. tornadoes and planetary circulation features that were obtained from reanalysis data. The ability of our model to simulate multiple-scale atmospheric phenomena opens the opportunity to study such teleconnection dynamically, which in turn will lead to a better understanding of convective storm activity, both for storm prediction and projection under external forcing (Cheng et al. 2022).

Acknowledgments

The authors thank Chih-Chi Hu for valuable discussions. This study is supported under awards NA18OAR4320123, NA19OAR0220146, and NA19OAR0220147 from the National Oceanic and Atmospheric Administration (NOAA), U.S. Department of Commerce. This project was additionally funded under the NOAA Research Global-Nest initiative.

Open Research

Model used in this study is available at https://github.com/NOAA-GFDL/SHiELD_build. Simulations presented in this study are available at https://doi.org/10.5281/zenodo.8428465.

References

Cheng, K.-Y., Harris, L., Bretherton, C., Merlis, T. M., Bolot, M., Zhou, L., et al. (2022). Impact of Warmer Sea Surface Temperature on the Global Pattern of Intense Convection: Insights From a Global Storm Resolving Model. Geophysical Research Letters, 49(16), e2022GL099796. https://doi.org/10.1029/2022GL099796

Davies-Jones, R. (2015). A review of supercell and tornado dynamics. Atmospheric Research, 158–159, 274–291. https://doi.org/10.1016/j.atmosres.2014.04.007

Gensini, V. A., Gold, D., Allen, J. T., & Barrett, B. S. (2019). Extended U.S. Tornado Outbreak During Late May 2019: A Forecast of Opportunity. Geophysical Research Letters, 46(16), 10150–10158. https://doi.org/10.1029/2019GL084470

Harris, L., Zhou, L., Kaltenbaugh, A., Clark, S., Cheng, K.-Y., & Bretherton, C. (2023). A Global Survey of Rotating Convective Updrafts in the GFDL X-SHiELD 2021 Global Storm Resolving Model. Journal of Geophysical Research: Atmospheres, 128(10), e2022JD037823. https://doi.org/10.1029/2022JD037823

Harris, L. M., Lin, S.-J., & Tu, C. (2016). High-Resolution Climate Simulations Using GFDL HiRAM with a Stretched Global Grid. Journal of Climate, 29(11), 4293–4314. https://doi.org/10.1175/JCLI-D-15-0389.1

Harris, L., Chen, X., Putman, W., Zhou, L., & Chen, J.-H. (2021). A Scientific Description of the GFDL Finite-Volume Cubed-Sphere Dynamical Core. https://doi.org/10.25923/6nhs-5897

Jeevanjee, N., & Zhou, L. (2022). On the Resolution-Dependence of Anvil Cloud Fraction and Precipitation Efficiency in Radiative-Convective Equilibrium. *Journal of Advances in Modeling Earth Systems*, *14*(3), e2021MS002759. https://doi.org/10.1029/2021MS002759

Judt, F., Klocke, D., Rios-Berrios, R., Vanniere, B., Ziemen, F., Auger, L., et al. (2021). Tropical Cyclones in Global Storm-Resolving Models. Journal of the Meteorological Society of Japan. Ser. II, 99(3), 579–602. https://doi.org/10.2151/jmsj.2021-029

Klemp, J. B., & Wilhelmson, R. B. (1978). The Simulation of Three-Dimensional Convective Storm Dynamics. Journal of the Atmospheric Sciences, 35(6), 1070–1096. https://doi.org/10.1175/1520-0469(1978)035<1070:TSOTDC>2.0.CO;2

346 Lin, S.-J. (1997). A finite-volume integration method for computing pressure gradient force in
347 general vertical coordinates. Quarterly Journal of the Royal Meteorological Society, 123(542),
348 1749–1762. https://doi.org/10.1002/qj.49712354214
349 Lin, S.-J. (2004). A "Vertically Lagrangian" Finite-Volume Dynamical Core for Global Models.
350 Monthly Weather Review, 132(10), 2293–2307. https://doi.org/10.1175/1520-
351 0493(2004)132<2293:AVLFDC>2.0.CO;2
352 Lin, S.-J., & Rood, R. B. (1997). An explicit flux-form semi-lagrangian shallow-water model on
353 the sphere. Quarterly Journal of the Royal Meteorological Society, 123(544), 2477–2498.
354 https://doi.org/10.1002/qj.49712354416
355 Markowski, P. M. (2002). Hook Echoes and Rear-Flank Downdrafts: A Review. Monthly
356 Weather Review, 130(4), 852–876. https://doi.org/10.1175/1520-
357 0493(2002)130<0852:HEARFD>2.0.CO;2
358 Markowski, P. M., & Richardson, Y. P. (2009). Tornadogenesis: Our current understanding,
359 forecasting considerations, and questions to guide future research. Atmospheric Research, 93(1),
360 3–10. https://doi.org/10.1016/j.atmosres.2008.09.015
361 Nesbitt, S. W., Salio, P. V., Ávila, E., Bitzer, P., Carey, L., Chandrasekar, V., et al. (2021). A
362 Storm Safari in Subtropical South America: Proyecto RELAMPAGO. Bulletin of the American
363 Meteorological Society, 102(8), E1621–E1644. https://doi.org/10.1175/BAMS-D-20-0029.1
364 Noda, A., & Niino, H. (2003). Critical grid size for simulating convective storms: A case study
365 of the Del City supercell storm. Geophysical Research Letters, 30(16).
366 https://doi.org/10.1029/2003GL017498

Nugent, J. M., Turbeville, S. M., Bretherton, C. S., Blossey, P. N., & Ackerman, T. P. (2022). Tropical Cirrus in Global Storm-Resolving Models: 1. Role of Deep Convection. Earth and Space Science, 9(2), e2021EA001965. https://doi.org/10.1029/2021EA001965

Orf, L., Wilhelmson, R., Lee, B., Finley, C., & Houston, A. (2016). Evolution of a Long-Track Violent Tornado within a Simulated Supercell. Bulletin of the American Meteorological Society, 98(1), 45–68. https://doi.org/10.1175/BAMS-D-15-00073.1

Potvin, C. K., & Flora, M. L. (2015). Sensitivity of Idealized Supercell Simulations to Horizontal Grid Spacing: Implications for Warn-on-Forecast. Monthly Weather Review, 143(8), 2998–3024. https://doi.org/10.1175/MWR-D-14-00416.1

Putman, W. M., & Lin, S.-J. (2007). Finite-volume transport on various cubed-sphere grids. Journal of Computational Physics, 227(1), 55–78. https://doi.org/10.1016/j.jcp.2007.07.022

Rotunno, R., Markowski, P. M., & Bryan, G. H. (2017). “Near Ground” Vertical Vorticity in Supercell Thunderstorm Models. Journal of the Atmospheric Sciences, 74(6), 1757–1766. https://doi.org/10.1175/JAS-D-16-0288.1

Satoh, M., Stevens, B., Judt, F., Khairoutdinov, M., Lin, S.-J., Putman, W. M., & Düben, P. (2019). Global Cloud-Resolving Models. Current Climate Change Reports, 5(3), 172–184. https://doi.org/10.1007/s40641-019-00131-0

Schlesinger, R. E. (1978). A Three-Dimensional Numerical Model of an Isolated Thunderstorm: Part I. Comparative Experiments for Variable Ambient Wind Shear. Journal of the Atmospheric Sciences, 35(4), 690–713. https://doi.org/10.1175/1520-0469(1978)035<0690:ATDNMO>2.0.CO;2

Schmidt, F., 1977: Variable fine mesh in the spectral global models. Beitr. Phys. Atmos., 50, 211–217.

390 Stevens, B., & Bony, S. (2013). What Are Climate Models Missing? Science, 340(6136), 1053–
391 1054. https://doi.org/10.1126/science.1237554
392 Stevens, B., Satoh, M., Auger, L., Biercamp, J., Bretherton, C. S., Chen, X., et al. (2019).
393 DYAMOND: the DYnamics of the Atmospheric general circulation Modeled On Non-
394 hydrostatic Domains. Progress in Earth and Planetary Science, 6(1), 61.
395 https://doi.org/10.1186/s40645-019-0304-z
396 Toy, M. D. (2012). A Supercell Storm Simulation Using a Nonhydrostatic Cloud-Resolving
397 Model Based on a Hybrid Isentropic-Sigma Vertical Coordinate. Monthly Weather Review,
398 141(4), 1204–1215. https://doi.org/10.1175/MWR-D-12-00215.1
399 Ullrich, P. A., Jablonowski, C., Kent, J., Lauritzen, P. H., Nair, R., Reed, K. A., et al. (2017).
400 DCMIP2016: a review of non-hydrostatic dynamical core design and intercomparison of
401 participating models. Geoscientific Model Development, 10(12), 4477–4509.
402 https://doi.org/10.5194/gmd-10-4477-2017
403 Wang, P. K., Cheng, K.-Y., Setvak, M., & Wang, C.-K. (2016). The origin of the gullwing-
404 shaped cirrus above an Argentinian thunderstorm as seen in CALIPSO images. Journal of
405 Geophysical Research: Atmospheres, 121(7), 2015JD024111.
406 https://doi.org/10.1002/2015JD024111
407 Weisman, M. L., & Klemp, J. B. (1982). The Dependence of Numerically Simulated Convective
408 Storms on Vertical Wind Shear and Buoyancy. Monthly Weather Review, 110(6), 504–520.
409 https://doi.org/10.1175/1520-0493(1982)110<0504:TDONSC>2.0.CO;2
410 Weisman, Morris L., & Rotunno, R. (2000). The Use of Vertical Wind Shear versus Helicity in
411 Interpreting Supercell Dynamics. Journal of the Atmospheric Sciences, 57(9), 1452–1472.
412 https://doi.org/10.1175/1520-0469(2000)057<1452:TUOVWS>2.0.CO;2

Wurman, J., Dowell, D., Richardson, Y., Markowski, P., Rasmussen, E., Burgess, D., et al. (2012). The Second Verification of the Origins of Rotation in Tornadoes Experiment: VORTEX2. Bulletin of the American Meteorological Society, 93(8), 1147–1170. https://doi.org/10.1175/BAMS-D-11-00010.1

Wurman, J., Kosiba, K., Robinson, P., & Marshall, T. (2013). The Role of Multiple-Vortex Tornado Structure in Causing Storm Researcher Fatalities. Bulletin of the American Meteorological Society, 95(1), 31–45. https://doi.org/10.1175/BAMS-D-13-00221.1

Zarzycki, C. M., Jablonowski, C., Kent, J., Lauritzen, P. H., Nair, R., Reed, K. A., et al. (2019). DCMIP2016: the splitting supercell test case. Geoscientific Model Development, 12(3), 879–892. https://doi.org/10.5194/gmd-12-879-2019

Zhao, M., Held, I. M., & Lin, S.-J. (2012). Some Counterintuitive Dependencies of Tropical Cyclone Frequency on Parameters in a GCM. Journal of the Atmospheric Sciences, 69(7), 2272–2283. https://doi.org/10.1175/JAS-D-11-0238.1

Zhou, L., Harris, L., Chen, J.-H., Gao, K., Guo, H., Xiang, B., et al. (2022). Improving Global Weather Prediction in GFDL SHiELD Through an Upgraded GFDL Cloud Microphysics Scheme. Journal of Advances in Modeling Earth Systems, 14(7), e2021MS002971. https://doi.org/10.1029/2021MS002971

Zavadoff, B. L., Gao, K., Lopez, H., Lee, S.-K., Kim, D., & Harris, L. M. (2023). Improved MJO Forecasts Using the Experimental Global-Nested GFDL SHiELD Model. Geophysical Research Letters, 50(6), e2022GL101622. https://doi.org/10.1029/2022GL101622